Low-Cost Sensors for Image based Measurement of 2D Velocity and Yaw Rate

Malte Joos, Julius Ziegler and Christoph Stiller

Department of Measurement and Control (MRT)
Karlsruhe Institute of Technology (KIT)
76131 Karlsruhe, Germany
malte.joos@student.kit.edu,{ziegler|stiller}@kit.edu

***Abstract*— Numerous applications require precise determination of the motion of a textured surface. Image based sensors are attractive for this purpose, since they are contactless and do not suffer from slip effects. Moreover, they do not only measure scalar speed, but can determine velocity as a 2d vectorial quantity, and, if two sensors are combined, can even observe yaw rate of the surface. If this kind of sensor is mounted inversely on a vehicle, it can determine its motion by measuring the relative displacement of the road surface. In this paper we will use a commercial motion sensor that has been originally designed for application in an optical computer mouse. We will show that, by well-considered dimensioning of the optical part of the system, this sensor can measure velocities in a range that is typical for automotive application. The result is a highly integrated, low-cost, angle sensitive motion sensor that does not exhibit slip effects. We evaluate this sensor through testing on a vehicle that is equipped with reference sensors, with special consideration on the advantages of this measurement principle over conventional wheel speed sensors.**

I. Introduction

Image based sensors for determining relative motion of a textured surface are well developed and find wide application in different domains. These include production lines for rolled goods like textile and paper, as well as velocity measurement for mobile robotic or automotive applications. As opposed to simpler means of velocity measurement, like encoder based wheel speed sensors, these sensors do not suffer from slip effects, and for this reason, have been used with success to observe the slip angle in automotive actuation[1][2][3].

Several methods to determine motion using an imaging sensor have been proposed. By exploiting the phenomenon of motion blur that occurrs when using long exposure times, the direction of motion can be determined even from a single image. By using modulated illumination of the tracking surface, both direction and magnitude of the velocity vector can be determined through analysis in the frequency domain [4]. An alternative approach are methods based on processing sequences of multiple images. These methods allow to determine both magnitude and direction of motion without a modulated light source. Changes between successive image frames are detected by image processing and the displacement vector is determined by homogeneous optical flow estimation [5]. Two well-known algorithms to measure the displacement of image features are shape context matching [6] and SIFT [7].

Since the 90s, image based motion detection has been applied in pointing devices for personal computers (optical mice). This application has lead to mass production of special purpose motion detection hardware, with the photo sensitive area and image processing hardware embedded on a single chip. Compared to setups consisting of conventional, high resolution CMOS cameras with separate processing hardware, these highly integrated devices typically only have a small photo sensitive area consisting of a few picture elements (pixels), but outpace the larger systems in terms of achievable frame rate.

In this work, a commercial motion sensor that has been designed for optical computer mice is used to create a low-cost optical sensor for measuring the velocity of an automobile. We will show that by fitting a macroscopic lens, the upper velocity bound of the sensor can be increased from 1 to 30 m/s, and the measuring distance from few mm to approximately 1 m.

The rest of this work is structured as follows: In section II, the sensor chip and its features are described. Further we will discuss the imaging properties of the sensor when combined with a specific lens. In section III we will derive the least square estimator for displacement and yaw rate that can be applied when two or more of the sensors are combined. Section IV sums up experimental results we obtained by mounting two of the sensors to a passenger car equipped with an inertial navigation system and wheel speed sensors as reference devices. We close the article with conclusions and an outlook on further research in section V.

II. Sensor specification

A. Optical mouse sensor

The optical mouse sensor used in this work is an ADNS-3080 manufactured by Avago Technologies [8]. Its main feature is a high achievable frame rate of up to 6469 frames per second (fps). Its photosensitive area is 1.7 by 1.7 mm at a resolution of 30 by 30 pixels. It produces gray scale images with 6 bit quantization (64 different gray scale values). The ADNS-3080 measures changes in position by optically acquiring sequential surface images (frames)

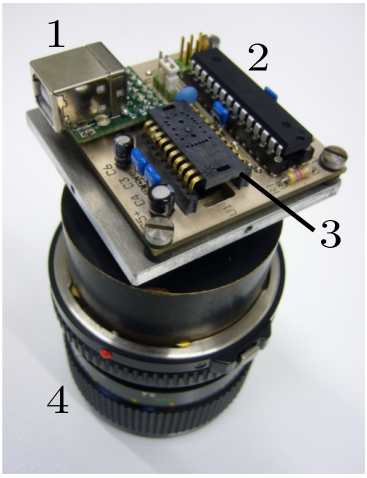

Fig. 1. The entire sensor: 1) USB device, 2) Microcontroller, 3) ADNS-3080, 4) Object lens.

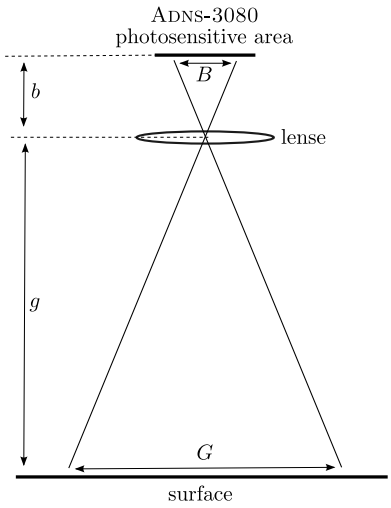

Fig. 2. Optical assembly

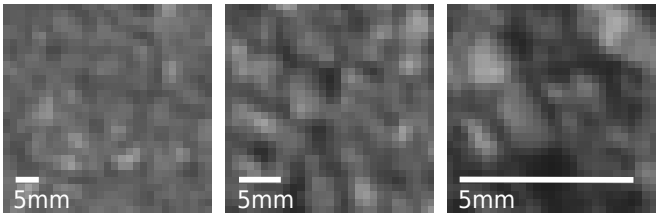

Fig. 3. Raw images of a road surface for different image regions.

and mathematically determining the direction and magnitude of movement through feature tracking. The sensor can be queried at any time for the displacement Δx and Δy that has occurred since the last query. The maximum velocity that the sensor can track when used with the purpose build plastic lens of the manufacturer is specified to 1 m/s.

By interfacing the sensor with a microcontroller circuit and a USB device, the full feature set of the sensor can be accessed (Fig. 1). Most importantly, this is the possibility to read out the raw data captured by the imager. Only by exploiting this feature, it becomes possible to calibrate an optical system fitted to the sensor, and to validate that the tracking surface is in focus. The sensor provides some additional feedback that can be used to tune operating parameters. These are mainly the number of valid features visible by the sensor in the current frame, the current overall frame rate and the shutter speed. The frame rate can be either set to a constant value or automatically adapted to lighting and surface conditions. To achieve a fast frame rate, the imaged surface has to be illuminated sufficiently.

Depending on the magnification of the employed object lens and the size of the acquired image region this sensor can be used for a large range of velocities. From microscopic dimensions with high sensitivity up to velocities of several hundred kilometers per hour. However, measurement uncertainty increases proportionally with the magnification.

B. Imaging properties

The assembly of the object lens and the ADNS-3080 relative to the surface is defined by four parameters: the focal length f of the object lens, the object- and image distance g and b respectively, and the image region G of the surface (Fig. 2).

The size B of the image is determined by the ADNS-3080 and constitutes 1.7 mm. The object distance g and the necessary image region G must be chosen to match the target speed (see below in (3)) and measuring distance. The resultant image distance b is given by the optical magnification

$$\frac{b}{g} = \frac{B}{G}. \tag{1}$$

To achieve a sharp image, the lens formula gives the required focal length f of the object lens

$$\frac{1}{b} + \frac{1}{g} = \frac{1}{f}. \tag{2}$$

Figure 3 shows raw images of the ADNS-3080 captured from a road surface. The sensor was mounted in different heights using the same object lens to capture image regions at different scales. At each scale, the images exhibit sufficient structure to enable image based motion detection. As will be shown below, the chosen image region proportionally affects the sensitivity of the sensor and the maximum measurable velocity.

The ADNS-3080 outputs its displacement in dimensionless counts, where one count equals the displacement of the image about one pixel. Because the captured surface is mapped to 30 by 30 pixels the sensitivity of the sensor is reciprocally proportional to the captured image region. This means that the displacement vector is quantified to steps of $\frac{1}{30}$ the size of the captured image region.

On the other hand, the size of the image region determines the maximum measurable velocity. Defining x as the minimum overlap of two consecutive frames necessary to successfully calculate a displacement, the following equation represents the relation between the side length of the image

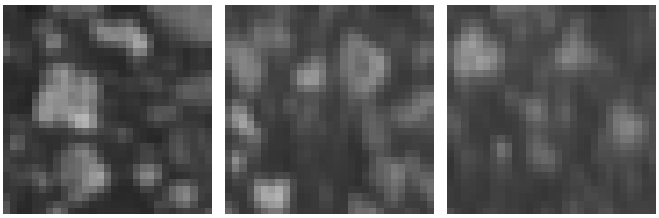

(a) 5 km/h (b) 30 km/h (c) 50 km/h

Fig. 4. Raw images of a road surface taken at different velocities. The image region is 30 by 30 mm.

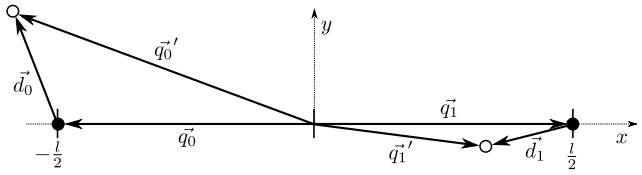

Fig. 5. Calculating yaw rate from two displacements.

region G, the frame rate r and therewith the maximum measurable velocity v_{max}:

$$G \cdot r \cdot (1 - x) = v_{max}. \tag{3}$$

In our test setup we captured 30 by 30 mm of the surface at a frame rate of 5000 fps. Using this setup, we successfully measured velocities of up to 30 m/s without reaching the limit v_{max}. From this, an upper bound for x can be estimated to 80%. In experiments performed on a roller type test stand, albeit with a different lens and a smaller field of view, minimum overlap x was determined to 65%. Transfering this to the optical setup on the car would yield a theoretical v_{max} of 68 m/s (186 km/h).

Fig. 4 shows raw images of a road surface taken at different velocities. The captured image region is 30 by 30 mm. One can see the incipient effect of motion blur for higher velocities. This effect can be reduced by shorter shutter speed or by increasing the distance of the sensor to the surface.

III. Determining translation and yaw rate

Assuming that two motion sensors are mounted on a rigid platform, not only the displacement, but also the yaw rate of the platform can be estimated. In this section we derive the least square estimator for overall displacement as well as yaw rate given the two noisy displacement measurements.

We will solve for the rotation angle $\hat{\theta}$ and translation $\hat{\vec{t}} = (\hat{t_x}, \hat{t_y})$ that, in a least square sense, best explains the noisy displacement measurements $\vec{d_0} = (\Delta x_0, \Delta y_0)$ and $\vec{d_1} = (\Delta x_1, \Delta y_1)$ picked up by the two sensors. We assume, without loss of generality, that the sensors are mounted at distance l and are initially arranged on the y-axis, symmetrically to the x-axis, at locations $\vec{q_0} = (-\frac{l}{2}, 0)$ and $\vec{q_1} = (\frac{l}{2}, 0)$ (Fig. 5). The observed, new positions of the sensors are

$$\vec{q_i'} = \vec{q_i} + \vec{d_i}, i \in \{0, 1\}.$$

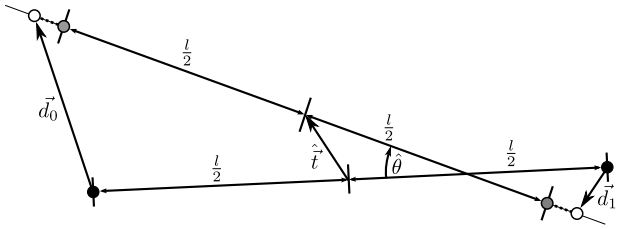

Fig. 6. Geometric interpretation of least square estimate. $\vec{d_0}$ and $\vec{d_1}$ are the noisy displacement measurements of the two sensors initially located at the black dots. The gray dots indicate the estimated new positions of the two sensors. The broken lines represent the errors that are minimized.

The observations are related to the parameters $\hat{\theta}$ and $\hat{\vec{t}}$ by the equation

$$\hat{\vec{q_i}} = \hat{R}\vec{q_i} + \hat{\vec{t}}, i \in \{0, 1\},$$

with $\hat{R}$ the estimated rotation matrix

$$\hat{R} = \begin{pmatrix} \cos(\hat{\theta}) & \sin(\hat{\theta}) \\ -\sin(\hat{\theta}) & \cos(\hat{\theta}) \end{pmatrix}.$$

The summed square error between estimate and observation is

$$e = \left\| \vec{q_0'} - \hat{\vec{q_0}} \right\|^2 + \left\| \vec{q_1'} - \hat{\vec{q_1}} \right\|^2.$$

The summed square error e can now be derived with respect to the parameters $\hat{\theta}$, $\hat{t_x}$ and $\hat{t_y}$:

$$\begin{aligned} \frac{\delta e}{\delta \hat{\theta}} &= (\Delta x_0 - \Delta x_1 - l) l \sin(\hat{\theta}) \\ &\quad + (\Delta y_0 - \Delta y_1) l \cos(\hat{\theta}) && (4) \\ \frac{\delta e}{\delta \hat{t_x}} &= 4\hat{t_x} - 2\Delta x_1 - 2\Delta x_0 && (5) \\ \frac{\delta e}{\delta \hat{t_y}} &= 4\hat{t_y} - 2\Delta y_1 - 2\Delta y_0 && (6) \end{aligned}$$

Setting (4)-(6) to zero and solving for the parameters yields the least square estimate:

$$\begin{aligned} \hat{\theta} &= \arctan\left(\frac{\Delta y_1 - \Delta y_0}{\Delta x_1 - \Delta x_0 + l}\right) && (7) \\ \hat{t_x} &= \frac{\Delta x_1 + \Delta x_0}{2} \\ \hat{t_y} &= \frac{\Delta y_1 + \Delta y_0}{2}. \end{aligned}$$

This solution has an intuitive geometric interpretation that is illustrated in Fig. 6. The translation vector $\hat{\vec{t}}$ is the average of the noisy displacements measured by the two sensors. It matches up the midpoints between the initial sensor positions and the sensor positions individually displaced by the measurements. The rotation angle $\hat{\theta}$ is the angle enclosed by the lines through the initial sensor positions and the displaced sensor positions.

Calculating Gauss' error propagation for equation 7 yields

$$\sigma_{\hat{\theta}} \approx \sqrt{2}\frac{\sigma_{\Delta x}}{l}, \tag{8}$$

suggesting that the uncertainty of angle measurement is reciprocal to the distance at which the sensors are placed.

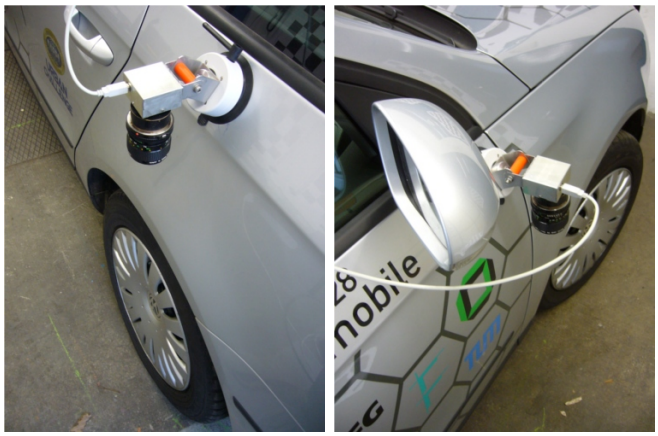

(a) Rear sensor (b) Front sensor

Fig. 7. The two sensors mounted on the car. One is mounted in the left rear and the other on the right front of the car.

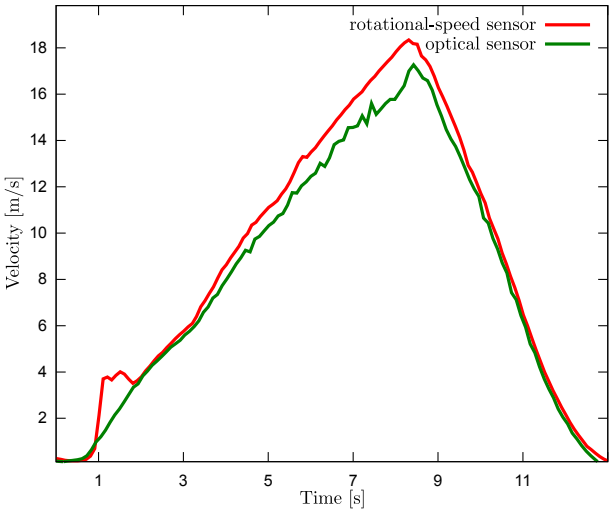

Fig. 8. Longitudinal velocity while acceleration and deceleration.

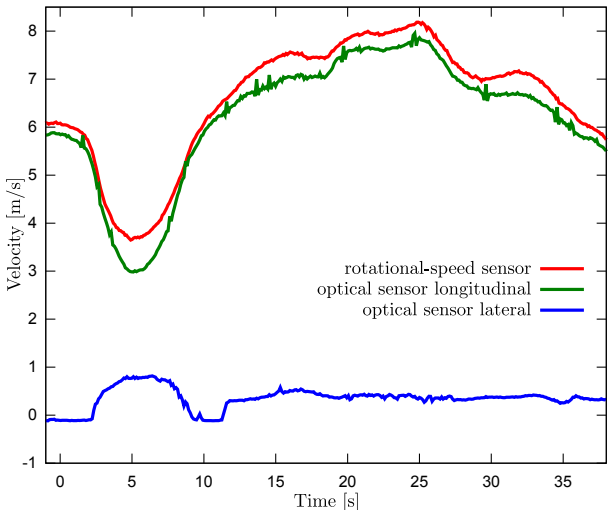

Fig. 9. Longitudinal and lateral velocity while cornering.

IV. Experimental results

We have tested the motion sensor on board of a passenger car (Volkswagen Passat). A reference velocity was obtained from the standard front wheel speed sensors of this car. A reference for yaw rate estimation is supplied by a high performance gyroscope included in the RT3000 inertial and GPS navigation system manufactured by Oxford Technical Solutions.

Due to rolling and pitching of the vehicle body, the distance between the sensor and the surface is not constant, resulting in measurement errors of the velocity. The velocity error is proportional to the relative deviation from the nominal height of the sensor. Hence, the effect can be minimized by increasing the distance of the sensor to the surface. By choosing a lens with a large focal length (50 mm), the distance from the surface could be increased to approximately 1 m. If a telecentric lens were used instead, the effect could be eliminated completely, since the magnification of such a lens is independent from the object distance. The experiments were carried out during day time in cloudy conditions, and no artificial lighting was used.

Fig. 7 shows two sensors mounted on the car. To increase precision of the yaw rate measurement, the sensors have been mounted at a maximum distance, along the diagonal of the car body, *cf.* also (8).

A. Non-slip velocity measurement

To demonstrate the advantage of non-slip measurement achievable with the optical sensor, the driven maneuver consisted of a phase of high acceleration with wheelspinning, followed by rapid deceleration. Fig. 8 shows the reference velocity of the wheel speed sensors and the measured longitudinal velocity of the optical sensor. One can see a raised velocity measurement of the wheel speed sensor due to wheelspinning in the beginning. The effect of wheelspinning can be seen over the entire process of acceleration.

The second notable feature of the image based sensor is its capability to determine true two dimensional motion. This was tested during a strong cornering maneuver with a slide in the beginning. In fig. 9, the reference velocity and both the longitudinal and lateral velocity measured by the optical sensor, are plotted over the same time axis. One can see the expected lateral velocity of the car during the slide as well as during the cornering which is not measurable by wheel speed sensors.

B. Yaw rate measurement using two sensors

The driven maneuver was a right turn followed by a slowly driven left turn followed by another faster driven left turn. Fig. 10 shows the estimated yaw rate of the motion sensors and the measured reference of the gyroscope. In addition, the longitudinal velocity of the car is shown below. The reference sensor only reports the absolute value of the yaw rate, hence, for easier comparison, the sign of the measurements of the image based sensor has been removed as well.

As one can see, there is a difference between the measured yaw rate and the reference, depending on the driven velocity and the turn direction. This dependency can be traced back to

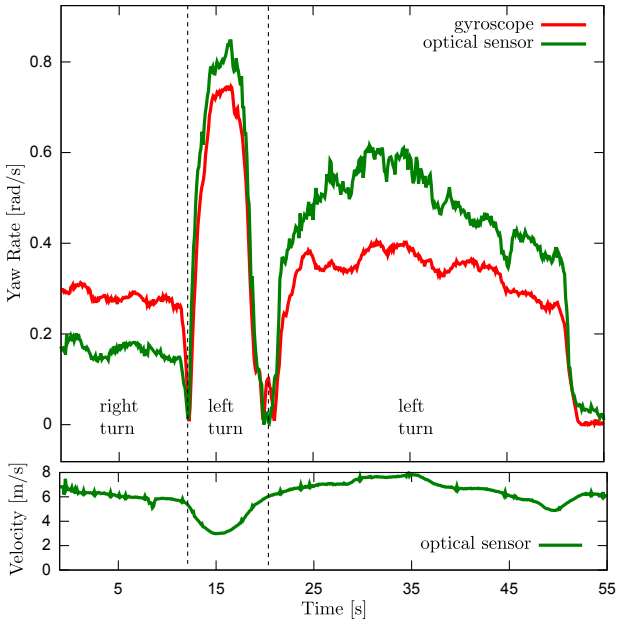

Fig. 10. Yaw rate during right turn followed by two left turns (top) and longitudinal velocity of the car (below).

rolling and pitching effects. Depending on the position where the sensors are mounted, acceleration (pitching) together with turning (rolling), leads to increasing and decreasing yaw rate measurements respectively. Here, in case of mounting the sensors diagonally, at the right front and left back of the car, the yaw rate measurement is damped for turning right, and amplified for turning left. The magnitude of this effect is coupled to the velocity and acceleration while turning. The car exhibits understeer and has a center of gravity well in front of its geometric center. This explains that the car tends to compress the suspension of the front wheels more than that of the rear wheels.

V. Conclusion and Future Work

With this work we have shown that a commercial, low cost optical mouse sensor can be used to measure speeds in excess of 30 m/s. The sensor is much smaller than PC based systems, measuring - without lens system - only 5 by 5 by 2.5 cm. While it probably cannot rival much larger and more expensive systems in terms of measurement precision, we believe it to be a good compromise for projects with budget or spatial constraints. Through a thorough analysis of the optical properties of the system it can, by mere adaption of the lens system, be scaled to almost arbitrary speeds and measuring distances. We are currently in the process of adapting the system to both a small robotic indoor platform that is based on a model car, and a sensor platform that is mounted on a conventional tramway.

One of the major issues in automotive application has been the unmodelled effects of rolling and pitching. We hope that, through a detailed model of suspension, their effects on yaw rate measurement can be minimized. An alternative would be to either employ a telecentric lens, or to explicitly measure the height of the sensor, using a dedicated, *e.g.* laser based, sensor.

VI. Acknowledgements

We gratefully acknowledge support of this work by the German research foundation (DFG) within the transregional collaborative research centre 28 “cognitive automobiles”.

References

[1] X. Song, Z. Song, L. Seneviratne, and K. Althoefer, “Optical flow-based slip and velocity estimation technique for unmanned skid-steered vehicles,” pp. 101 –106, sept. 2008.

[2] G. Reina, G. Ishigami, K. Nagatani, and K. Yoshida, “Vision-based estimation of slip angle for mobile robots and planetary rovers,” pp. 486 –491, may 2008.

[3] “Corrsys-datron optical sensors.” `http://www.corrsys-datron.com`.

[4] J. Horn, “Analysis of impulse train illuminated images for 2d velocity measurement,” vol. 3, pp. 1859 – 1862 Vol. 3, oct. 2004.

[5] J. Horn, *Two dimensional velocity measurement of textured surfaces by planar image sensors*. PhD thesis, Karlsruhe Institute of Technology, 2006.

[6] S. Belongie, J. Malik, and J. Puzicha, “Shape matching and object recognition using shape contexts,” *Pattern Analysis and Machine Intelligence, IEEE Transactions on*, vol. 24, pp. 509 –522, apr 2002.

[7] D. G. Lowe, “Distinctive image features from scale-invariant keypoints,” *International Journal of Computer Vision*, vol. 60, pp. 91–110, 2004.

[8] “Adns-3080 datasheet.” `http://www.avagotech.com`.